Supporting Information for

Solvent-dependent Self-assemblies with Multi-inverted Circularly Polarized Luminescence Based on 9,10-Distyrylanthracene

Meng Wang, Yuxuan Song, Zhixuan Wang, Bin Xu* and Wenjing Tian*

[a] *State Key Laboratory of Supramolecular Structure and Materials, College of Chemistry, Jilin University, Changchun 130012, P. R. China.*

E-mail: xubin@jlu.edu.cn, wjtian@jlu.edu.cn

Contents

1. Synthesis and characterization.

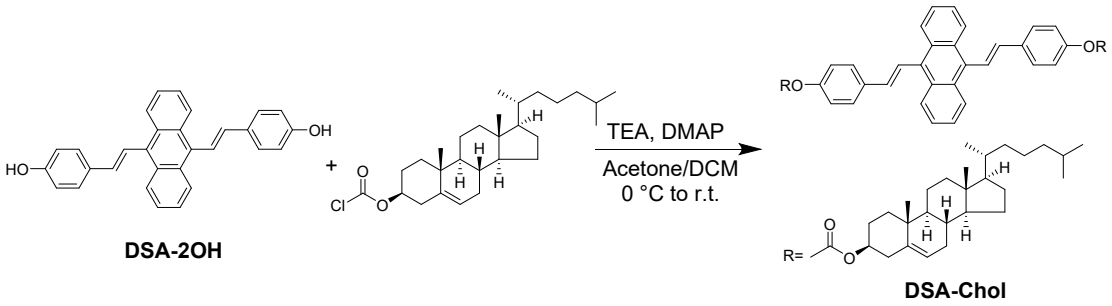

Synthesis method of DSA-2OH was referred to in previous work.[1] DSA-2OH (414 mg, 1 mmol), triethylamine (TEA, 3.3 mL), and 4-dimethylaminopyridine (DMAP, 10 mg) were dissolved in acetone (35 mL). The mixture was stirred under ice bath for 10 min. Subsequently, cholesteryl chloroformate (1.57 g, 3.5 mmol) was dissolved in 40 mL of dichloromethane (DCM), and the solution was added dropwise to the above mixture under stirring at 0 °C. Then the mixture was naturally warmed to room temperature and reacted for 8 h, with the reaction progress monitored by TLC. After the reaction was finished, the solvent was removed by rotary evaporation. The product was dissolved in chloroform, and the solution was washed sequentially with 1 M HCl, saturated brine, and water. The organic phase was dried over anhydrous $MgSO_4$. Then the $MgSO_4$ was removed by filtration, and the crude product was purified by column chromatography (silica gel, eluent: petroleum ether:DCM = 3:1 to 1:1). The target product DSA-Chol was obtained as a yellow solid powder (0.69 g, yield: 55.7%).

^{1}H NMR (500 MHz, Chloroform-*d*), see Figure. S21 : δ 8.42 – 8.33 (m, 4H), 7.89 (d, *J* = 16.4 Hz, 2H), 7.74 – 7.66 (m, 4H), 7.49 (dt, *J* = 6.9, 3.5 Hz, 4H), 7.32 – 7.27 (m, 4H), 6.92 (d, *J* = 16.5 Hz, 2H), 5.45 (dt, *J* = 4.5, 2.1 Hz, 2H), 4.63 (tt, *J* = 10.9, 5.1 Hz, 2H), 2.53 (tdd, *J* = 13.6, 9.1, 4.0 Hz, 4H), 2.14 – 1.70 (m, 13H), 1.66 – 0.80 (m, 63H), 0.70 (s, 6H).

^{13}C NMR (126 MHz, Chloroform-*d*), see Figure. S22 : δ 152.94, 150.87, 139.17, 136.42, 135.14, 132.54, 129.56, 127.56, 126.40, 125.50, 125.36, 123.25, 121.52, 78.99, 56.71, 56.15, 50.02, 42.34, 39.74, 39.53, 37.99, 36.87, 36.59, 36.20, 35.80,

31.94, 31.87, 28.24, 28.03, 27.70, 24.30, 23.84, 22.83, 22.57, 21.08, 19.32, 18.73, 11.88.

MALDI-TOF-MS, see Figure. S23 :m/z calcd. for $C_{86}H_{110}O_6$ $[M+H]^+$ 1239.84, found: 1239.80.

2. Experimental methods.

Materials. Except the DSA-2OH, all chemicals and solvents were used without further purification. Cholesteryl chloroformate, triethylamine (TEA) and 4-dimethylaminopyridine (DMAP) were purchased from TCI. Dichloromethane (DCM), petroleum ether and methanol used in synthesis were purchased from Shanghai Titan Scientific Co., Ltd. Acetone, hydrochloric acid and chloroform were purchased from Jilin Haodi Chemical Reagents Distribution Co., Ltd. Mg_2SO_4 was purchased from Tianjin Guangfu Technology Development Co., Ltd. Tetrahydrofuran (THF) and methanol used for assembly were both of spectroscopic grade and purchased from Shanghai Aladdin Biochemical Technology Co., Ltd. All the water used in the experiment and measurement was Milli-Q water (18.2 MΩ·cm).

Assembly sample preparation. 10.0 mg DSA-Chol sample was dispersed into 10 mL of spectroscopic grade THF as a stock solution. Taking the preparation of DSA-Chol in THF-H_2O (f_w = 80%, v/v) as an example. 1 mL stock solution was added in a 20 mL vials, and 1mL THF and 8 mL water were added into the solution in turn. The mixture was ultrasonicated for five minutes and subsequently allowed to stand for more than 1 hour to complete the assembly process ([DSA-Chol] = 8.07×10^{-5} mol/L).

Single crystal preparation. The DSA-Chol single crystal were obtained through solvent evaporation method in dichloromethane/acetone/methanol mixed solvent.

Density functional theory (DFT) computation. DFT and time-dependent density functional theory (TD-DFT) calculations were performed by Gaussian 16W program at B3LYP 6-311G(d) and CAM-B3LYP/6-31G(d) levels, respectively.

Ultraviolet-visible absorption spectra. The samples were recorded on a Shimadzu UV-2550 spectrophotometer.

Fluorescence spectra. The fluorescence spectra were recorded on a Shimadzu RF-5301 PC spectrometer. The width of the excitation and emission slits were 1.5 nm and the excitation wavelength (λ_{ex}) was 400 nm.

Fluorescence quantum yields. The samples were tested on a FLS980-S2S2-stm steadystate transient fluorescence spectrometer by using an integrating sphere.

NMR spectra. ^{1}H NMR, ^{13}C NMR spectra were recorded on a Bruker AVANCE III 500MHz system.

Mass spectra. Mass spectrum data were obtained by using a Kratos MALDI-TOF mass system.

Scanning electron microscopy (SEM). Solution aggregates were cast on a silicon wafer. After being dried in air, the sample was coated with a thin layer of Pt to enhance the electrical conductivity. Then the sample was imaged using a Hitachi Regulus8100 UHR FE-SEM or a Hitachi SU8020 CFE-SEM with an accelerating voltage of 3.0 kV and an operating current of 10 μA.

Transmission electron microscopy (TEM). Solution aggregates were dropped on a pure carbon film-coated copper grid and air-dried before measurement. Then the sample was imaged using a JEOL JEM-2100F instrument with an accelerating voltage of 120 kV.

Atomic force microscopy (AFM). Solution aggregates were cast on a mica wafer. After being dried in air, the sample was imaged using a Bruker ICON-XR instrument.

Circular dichroism (CD) spectra. CD spectra were measured using a JASCO J-1700 CD spectrometer at a scanning rate of 200 nm/min.

Circularly polarized luminescence (CPL) spectra. CPL spectra were measured using a JASCO CPL-300 spectrophotometer at a scanning rate of 200 nm/min. CPL spectra were converted to g_{lum} spectra using SpectraManager (JASCO) software. Each sample was tested several times by rotating to 0°, 90°, and 180° angles.

Single crystal X-ray diffraction. Single-crystal X-ray diffraction data were collected using synchrotron radiation and MAR325 CCD detector at Shanghai Synchrotron Radiation BL17B Beamline. The crystal structure was solved with SHELXT-2014/7 (Sheldrick, 2015) and refined using SHELXL-2014/7 (Sheldrick, 2015). Molecular graphics and publication materials were prepared with Bruker SHELXTL. The measurement method employed phi and omega scans. The completeness was low at 89.3% due to the data collection strategy as the space group was found to be *P*1. The crystals were difficult to obtain and the data had to be collected at a synchrotron, however the data is sufficient to confirm the proposed structure.

Powder X-ray diffraction (PXRD). PXRD analysis was performed on a Rigaku SmartLab 3 diffractometer with Cu/Kα radiation (λ = 1.5406 Å), which was operated at a voltage of 40 kV and a current of 30 mA. Samples were prepared on glass wafers and air-dried for PXRD testing.

Fourier transform infrared (FT-IR). FT-IR spectra were recorded on a Bruker VERTEX 80V FT-IR spectrometer. The sample was ground into powder and dried, then mixed with dried KBr (powder) and pressed into piece.

3. Supplementary figures.

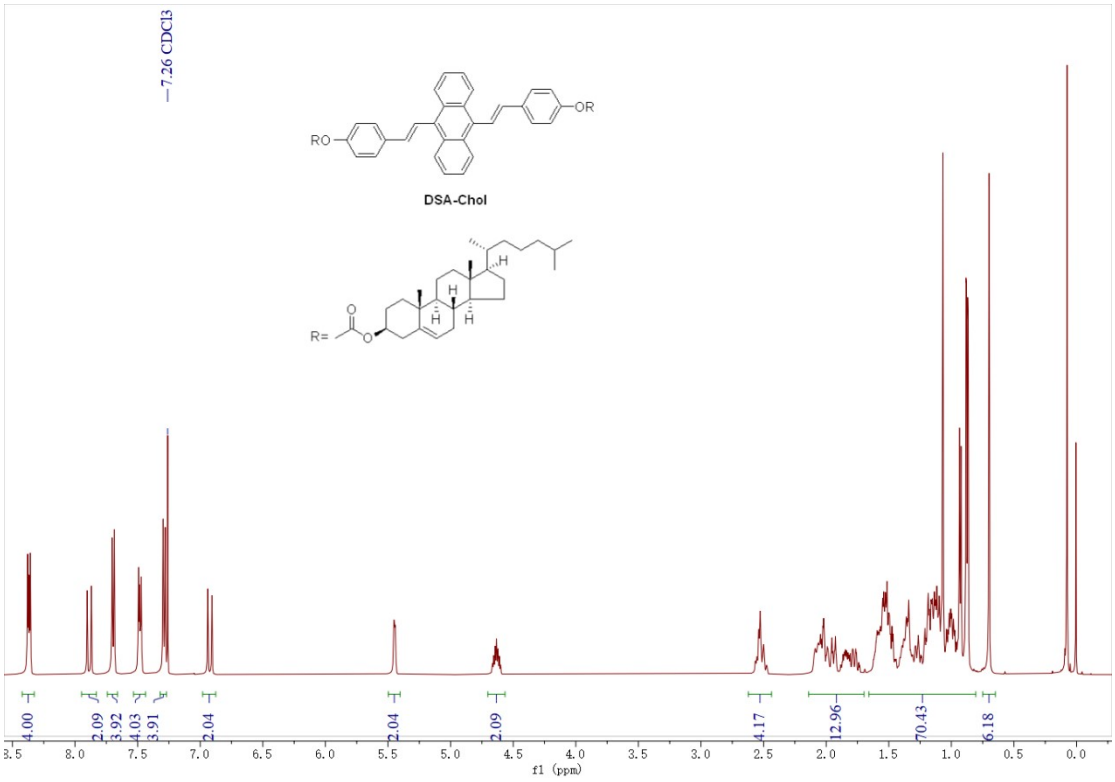

Fig. S1 ^{1}H-NMR spectrum of DSA-Chol.

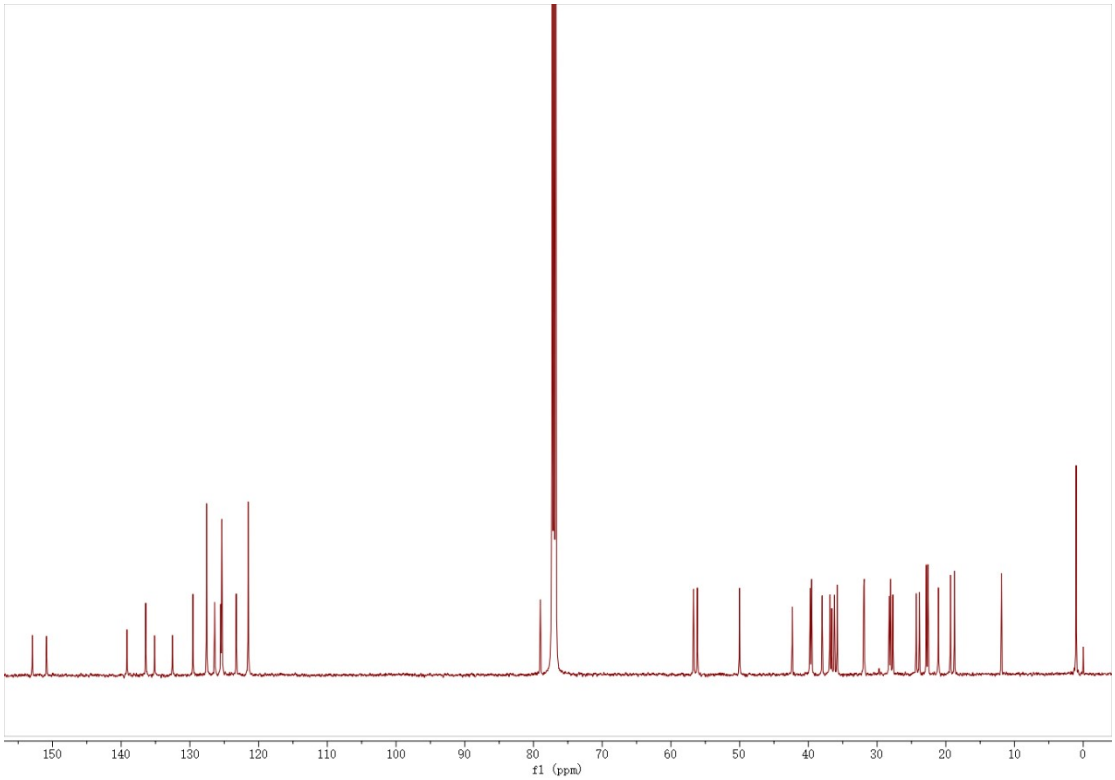

Fig. S2 ^{13}C-NMR spectrum of DSA-Chol.

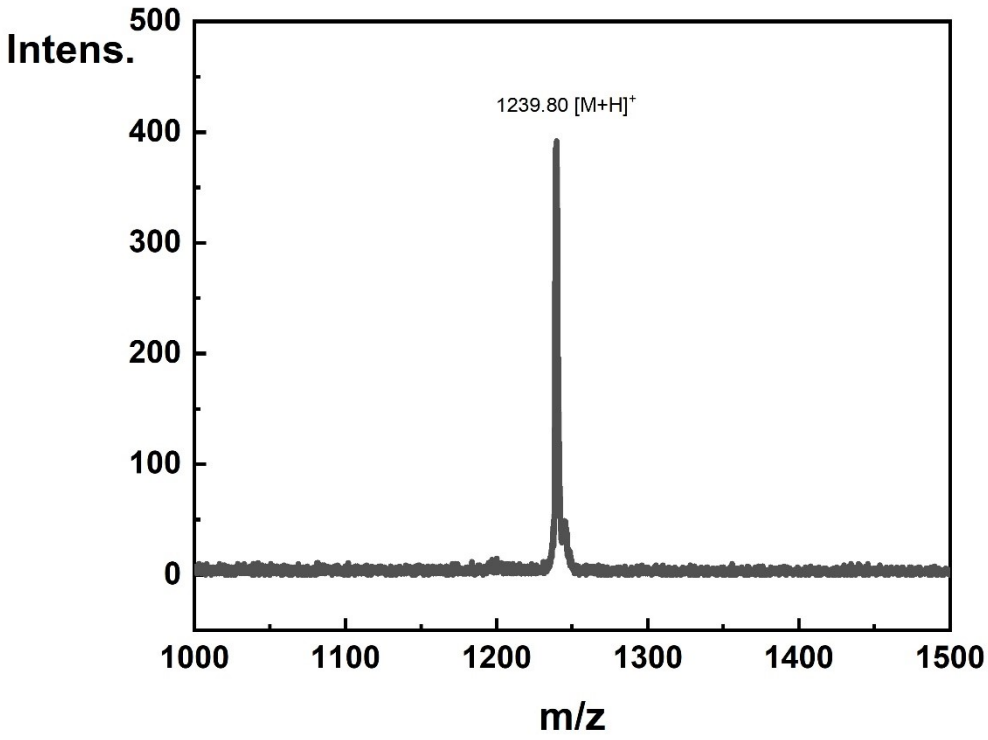

Fig. S3 MALDI-TOF-MS spectrum of DSA-Chol.

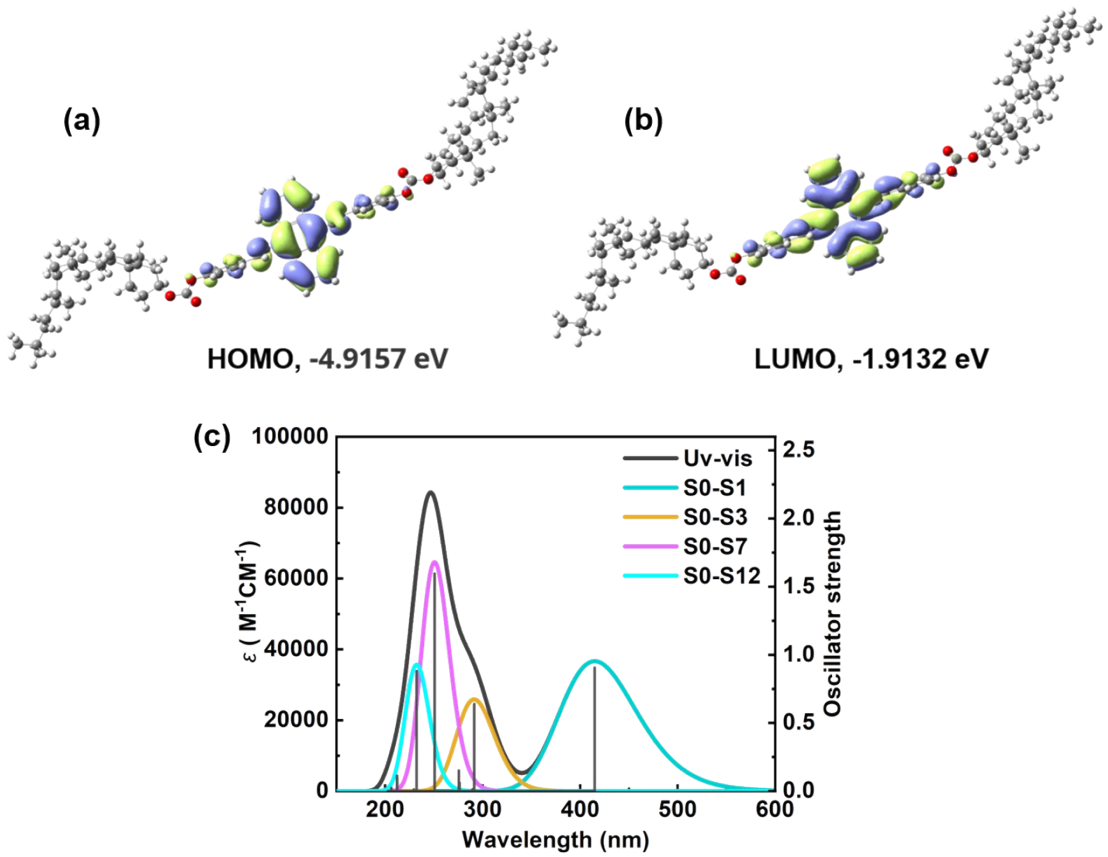

Fig. S4 (a) and (b) Frontier molecular orbitals of DSA-Chol calculated by DFT at B3LYP/6-311G(d,p) level.[2] The carbon, hydrogen and oxygen atoms are represented by gray, white and red balls, respectively. (c) Calculated UV-vis spectrum of DSA-Chol (black line) and contributions of different transitions. TD-DFT at CAM-B3LYP/6-31G(d) level. The data was analysed with the help of Multiwfn program.[3]

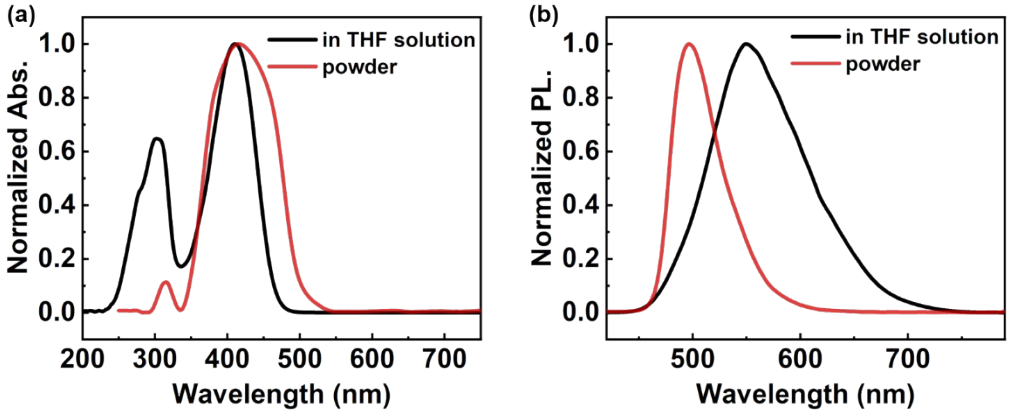

Fig. S5 Experimental (a) absorption spectra and (b) fluorescence spectra of DSA-Chol in powder state and in dilute THF solution ([DSA-Chol] = 8.07 × 10^{-5} mol/L).

(a)

(b)

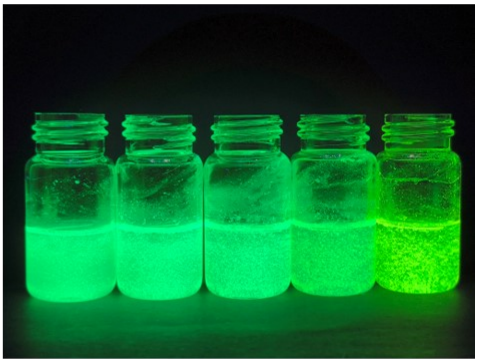

(c)

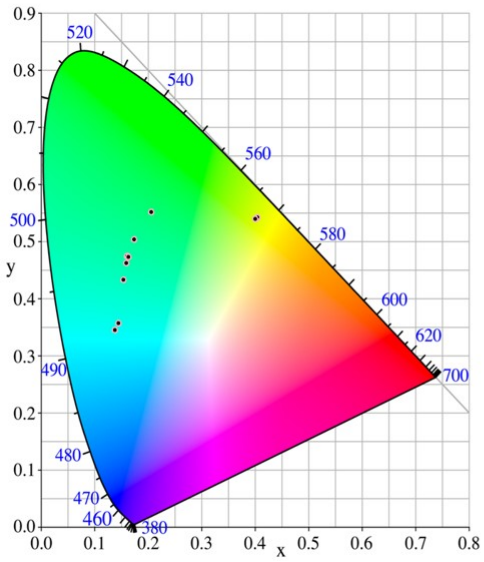

(d)

f_w(%)	CIE x	CIE y
0	0.4041	0.5431
10	0.4003	0.5404
20	0.1434	0.3567
30	0.137	0.3454
40	0.1532	0.4334
50	0.1602	0.4743
60	0.1592	0.463
70	0.1621	0.4735
80	0.1739	0.5046
90	0.2048	0.5522

Fig. S6 Fluorescence images of DSA-Chol assemblies in the aqueous system under 365 nm UV lamp irradiation: (a) f_w ranging from 0 to 40% (from left to right); (b) f_w ranging from 50% to 90% (from left to right). (c) CIE diagram and (d) xy coordinates of the emission colors at excitation wavelength of 400 nm (λ_{ex} = 400 nm).

Table. S1 Fluorescence quantum yields (QY or Φ) at different water fractions.

f_w(%)	Φ(%)[a]
dilute solution	19.31
0	18.71
10	15.06
20	21.53
30	28.5
40	24.55

50	31.82
60	24.99
70	24.95
80	18.79
90	20.67

[a] [DSA-Chol] = 8.07 × 10^{-5} M in THF/H_2O mixture (v/v).

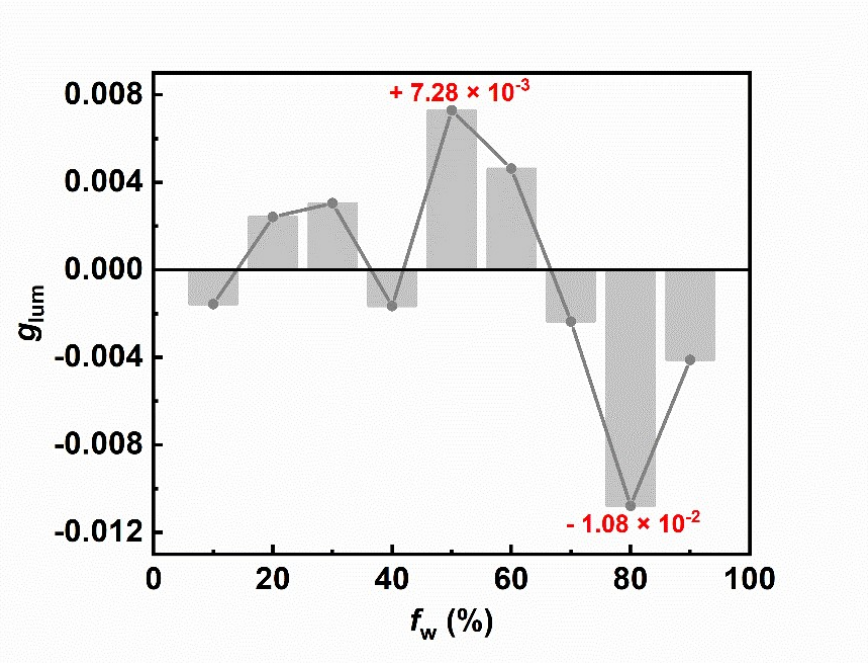

Fig. S7 Changes of the maximum g_{lum} values at different water fractions.

Table. S2 The maximum g_{lum} values at different water fractions.

f_w (%)	g_{lum} [a]
10	- 0.00158 (at 626 nm)
20	0.00241
30	0.00304
40	- 0.00166
50	0.00728
60	0.00462
70	- 0.00237

80	-0.01079
90	- 0.00412

[a] Measured at the maximum signal.[4]

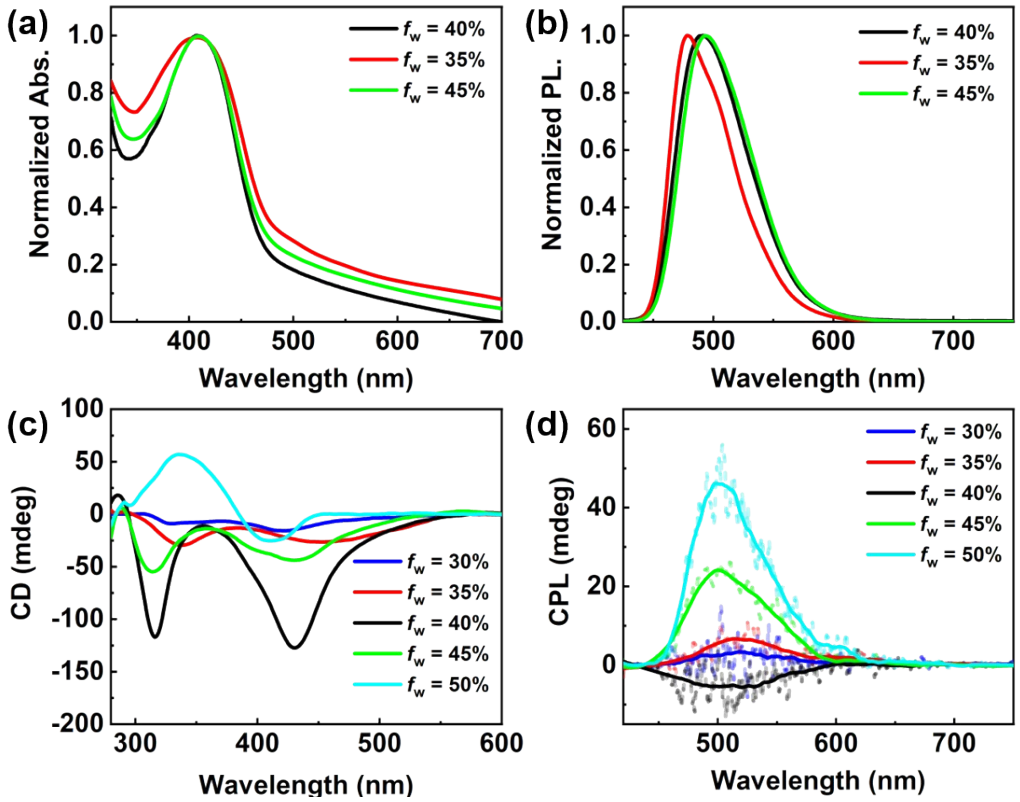

Fig. S8 (a) Absorption spectra and (b) fluorescence spectra of DSA-Chol in THF/H_2O at f_w = 35-45%. (c) CD spectra and (b) CPL spectra of DSA-Chol in THF/H_2O at f_w = 30-50%.

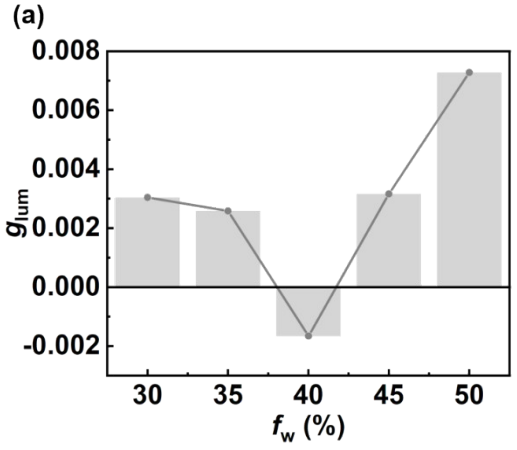

(b)

f_w(%)	g_{lum}[a]
30	0.00304 (at 502.5 nm)
35	0.00258 (at 525 nm)
40	- 0.00166
45	0.00316
50	0.00728

[a] Measured at the maximum signal.

Fig. S9 (a) Changes and (b) specific values of the maximum g_{lum} at f_w = 30-50%.

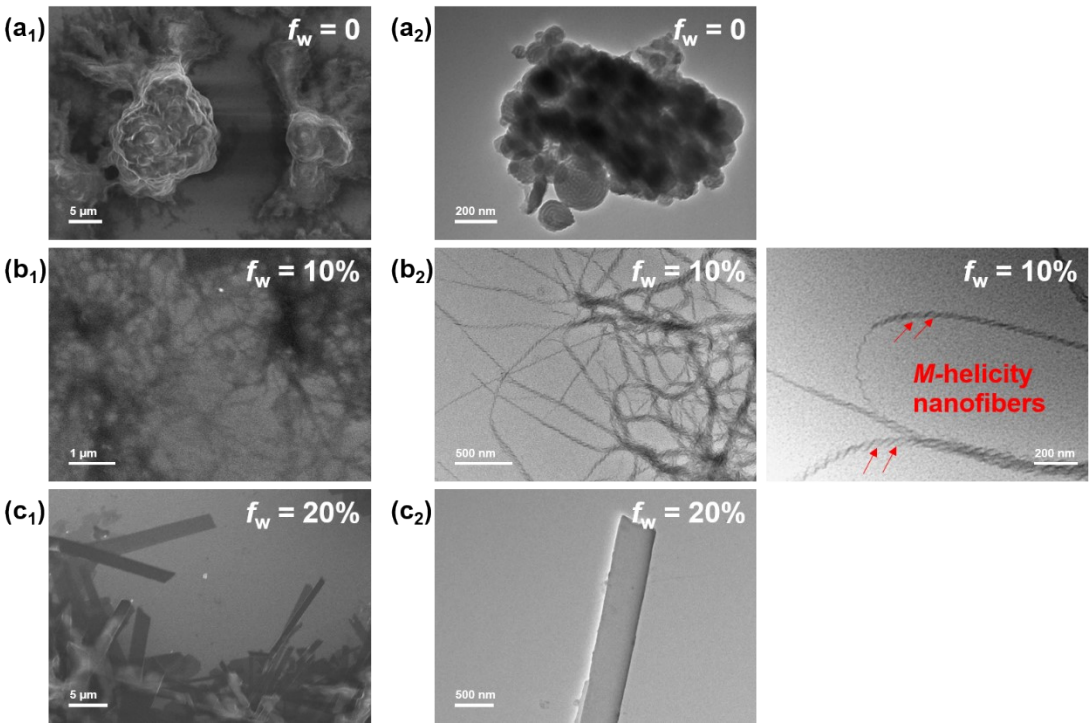

Fig. S10 (a_1) SEM image and (a_2) TEM image of DSA-Chol assemblies at f_w = 0. (b_1) SEM image and (b_2) TEM images of DSA-Chol assemblies at f_w = 10%. The nanofibers are difficult to observe under SEM possibly due to the poor conductivity of the assemblies. (c_1) SEM image and (c_2) TEM image of DSA-Chol assemblies at f_w = 20%.

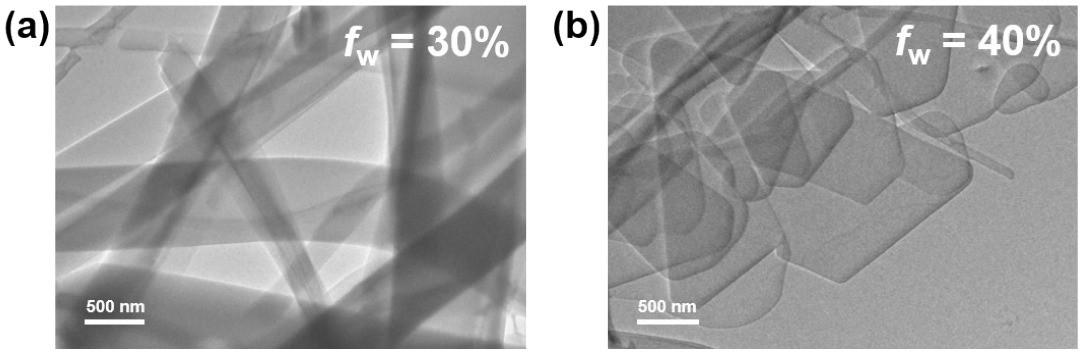

Fig. S11 TEM images of DSA-Chol assemblies at (a) f_w = 30% and (b) f_w = 40%.

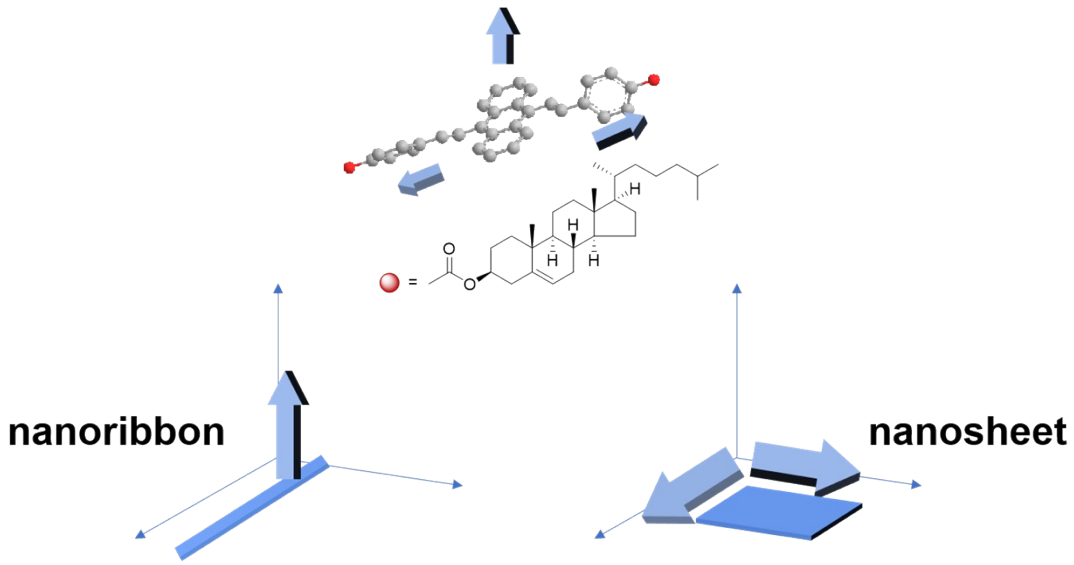

Fig. S12 Schematic diagram of two spatial packing orientations of DSA-Chol molecules.

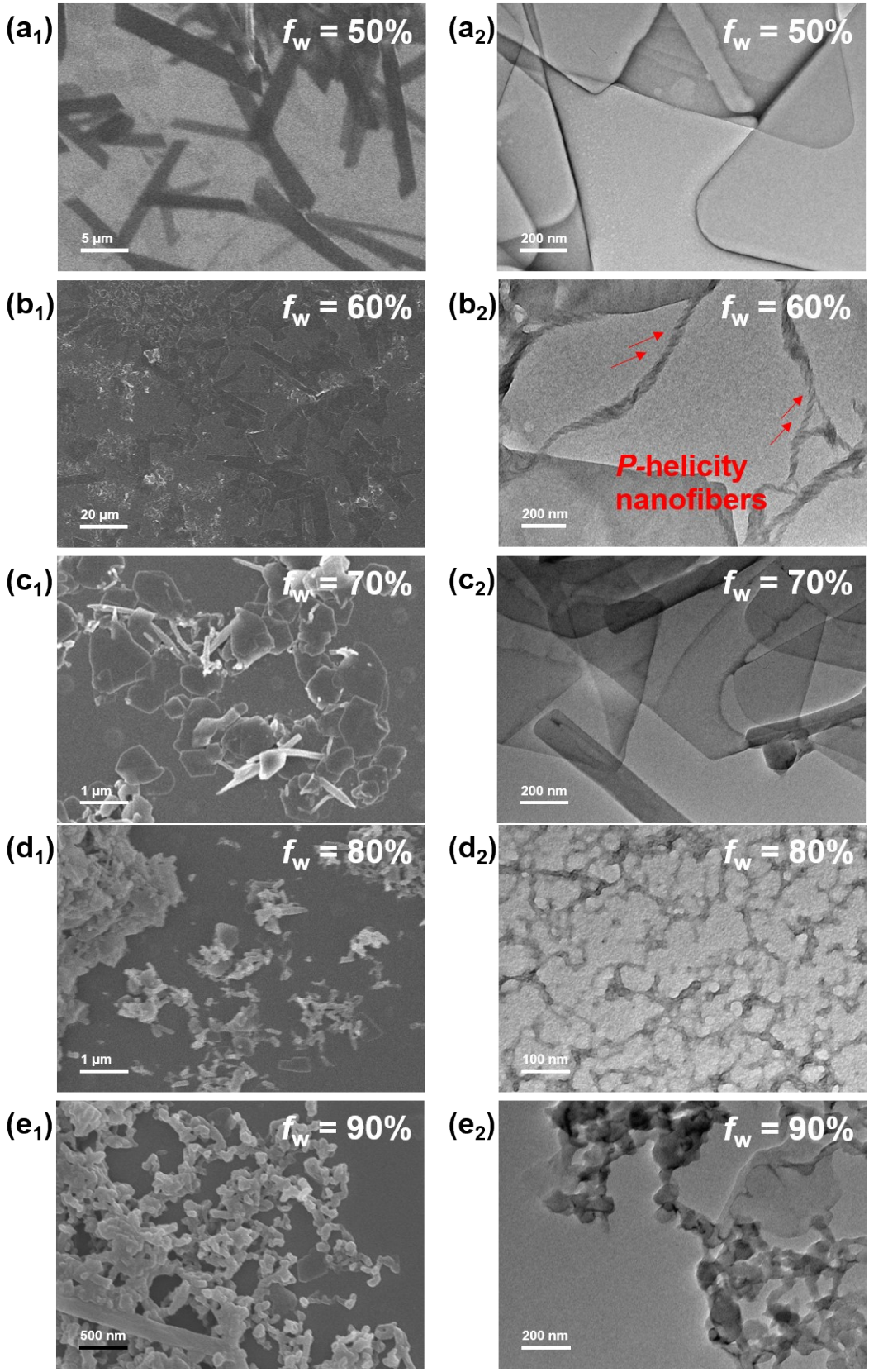

Fig. S13 SEM images of DSA-Chol assemblies at (a_1) f_w = 50%, (b_1) f_w = 60%, (c_1) f_w = 70%, (d_1) f_w = 80% and (e_1) f_w = 90%. TEM images of DSA-Chol assemblies at (a_2) f_w = 50%, (b_2) f_w = 60%, (c_2) f_w = 70%, (d_2) f_w = 80% and (e_2) f_w = 90%.

(a)

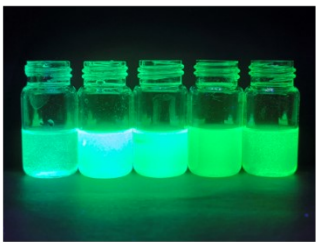

(b)

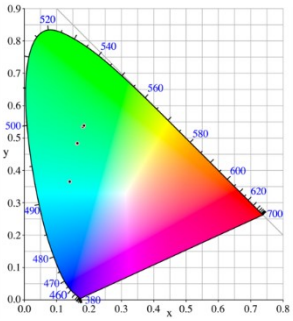

(c)

f_m(%)	CIE x	CIE y
50	0.1401	0.3652
60	0.1625	0.4825
70	0.1642	0.4837
80	0.1814	0.5349
90	0.1839	0.5388

Fig. S14 (a) Fluorescence image of DSA-Chol assemblies in the methanol system under 365 nm UV lamp irradiation, with f_m ranging from 50% to 90% (from left to right). (b) CIE diagram and (c) xy coordinates of the emission colors at excitation wavelength of 400 nm (λ_{ex} = 400 nm).

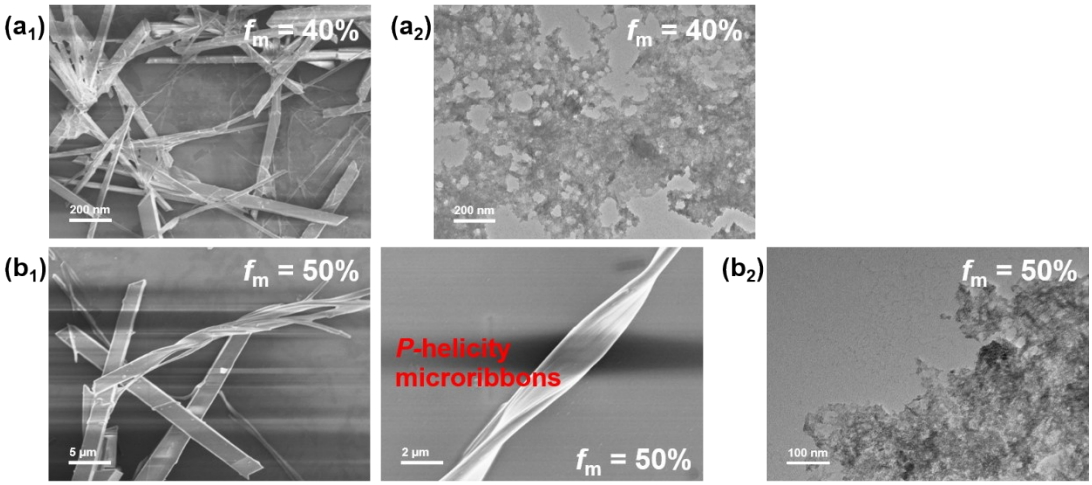

Fig. S15 (a_1) SEM image and (a_2) TEM image of DSA-Chol assemblies at f_m = 40%. (b_1) SEM images and (b_2) TEM image of DSA-Chol assemblies at f_m = 50%.

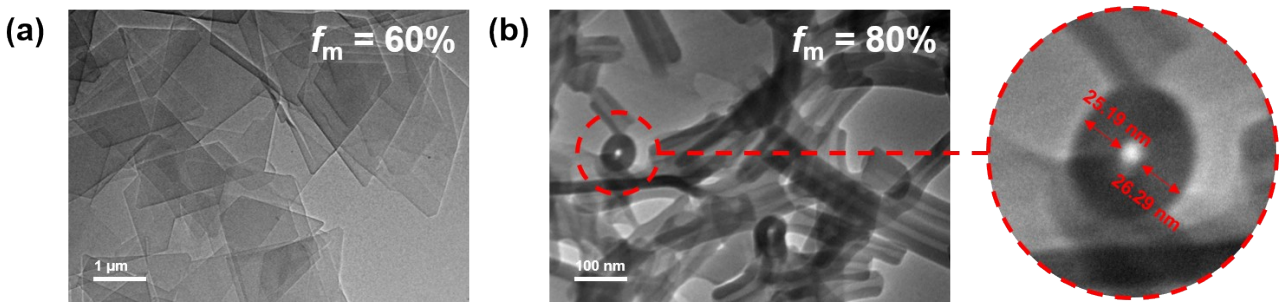

Fig. S16 TEM images of DSA-Chol assemblies at (a) f_m = 60% and (b) f_m = 80%.

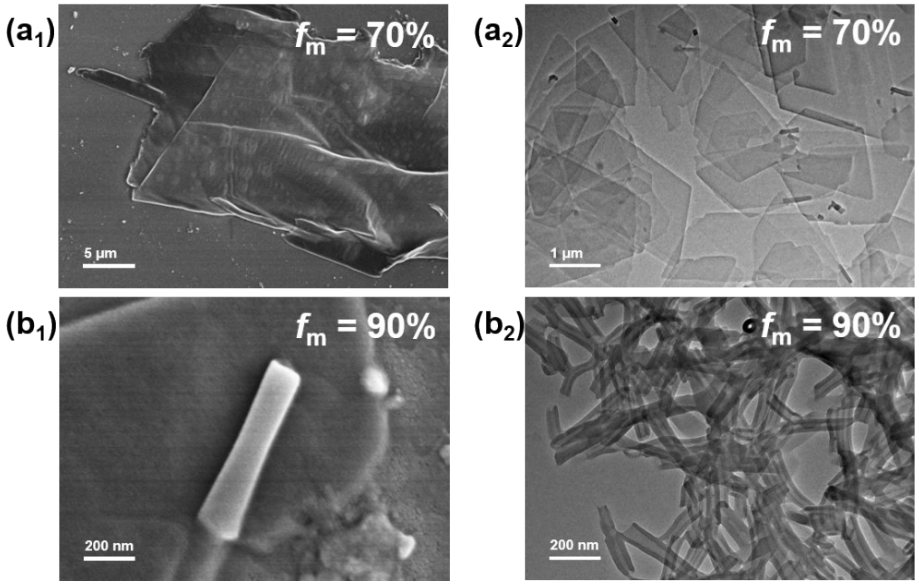

Fig. S17 (a_1) SEM image and (a_2) TEM image of DSA-Chol assemblies at f_m = 70%. (b_1) SEM image and (b_2) TEM image of DSA-Chol assemblies at f_m = 90%.

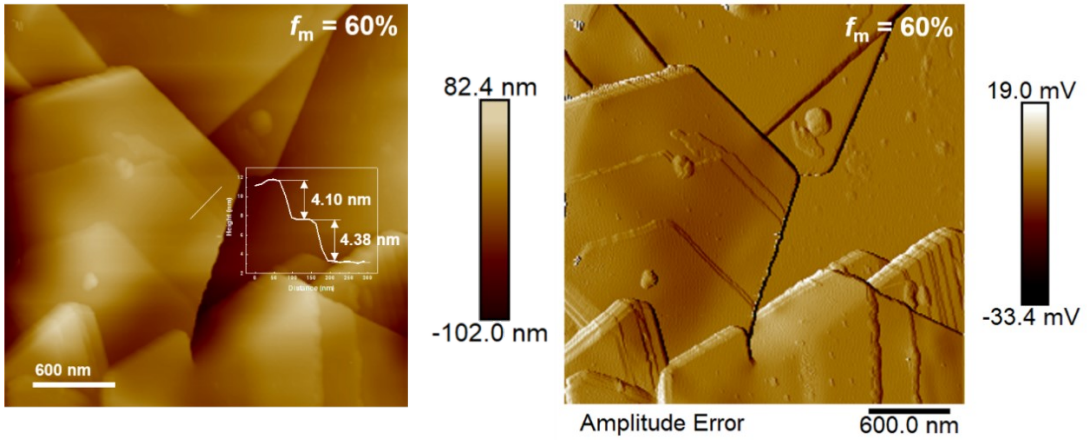

Fig. S18 AFM images of DSA-Chol assemblies at f_m = 60%.

(a)

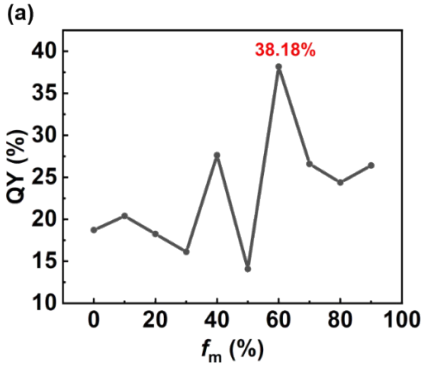

(b)

f_m(%)	Φ(%)[a]
0	18.71
10	20.38
20	18.25
30	16.12
40	27.62
50	14.08
60	38.18
70	26.59
80	24.38
90	26.40

[a] [DSA-Chol] = 8.07×10^{-5} M in THF/methanol mixture (v/v).

Fig. S19 (a) Changes and (b) specific values of the fluorescence quantum yields of DSA-Chol in THF/methanol system.

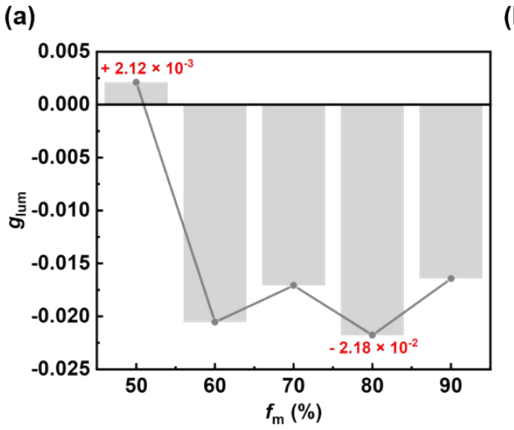

(b)

f_m(%)	g_{lum}[a]
50	0.00212 (at 476 nm)
60	- 0.02055
70	- 0.01709
80	- 0.02177
90	- 0.01645

[a] Measured at the maximum signal.

Fig. S20 (a) Changes and (b) specific values of the maximum g_{lum} at f_m = 50-90%.

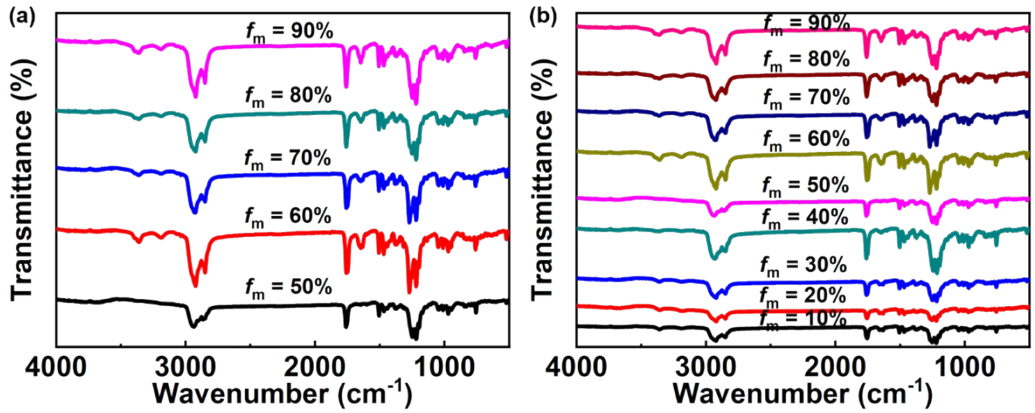

Fig. S21 (a) Stacked FT-IR spectra of DSA-Chol assemblies at f_m = 50-90%. (b) Stacked FT-IR spectra of DSA-Chol assemblies in THF/methanol system.

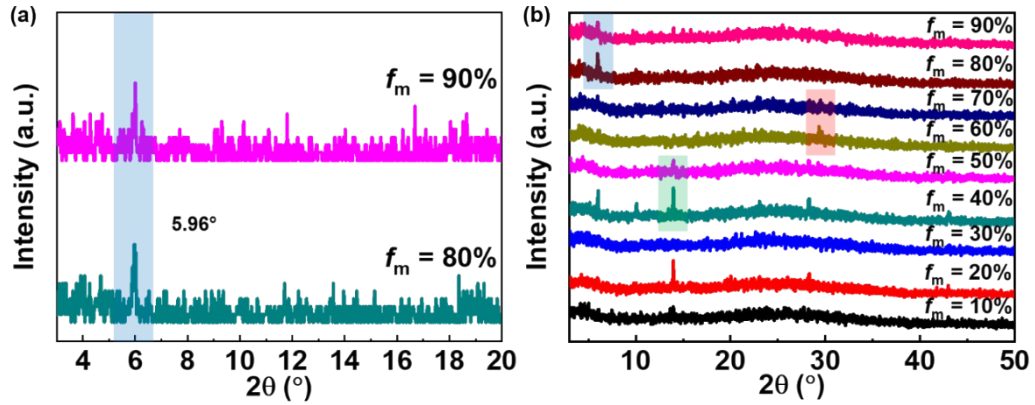

Fig. S22 (a) Small-angle stacked PXRD patterns of DSA-Chol assemblies at f_m = 80% and 90%. (b) Stacked PXRD patterns of DSA-Chol assemblies in THF/methanol system.

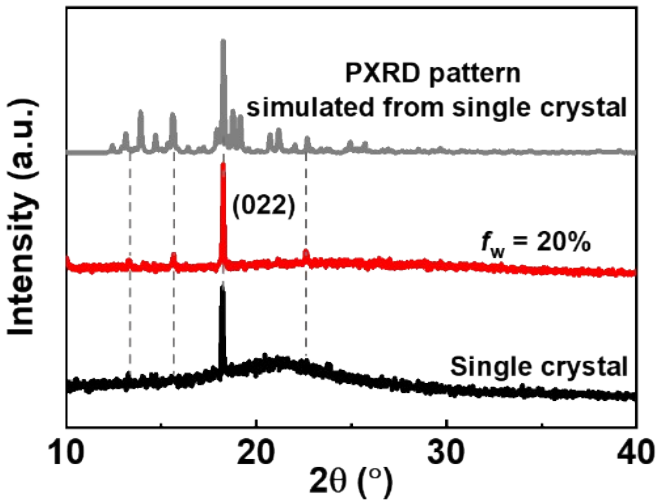

Fig. S23 PXRD patterns for the experimental single crystal (black line), those simulated from single-crystal data (gray line), and the assembly system with 20% water content (red line).

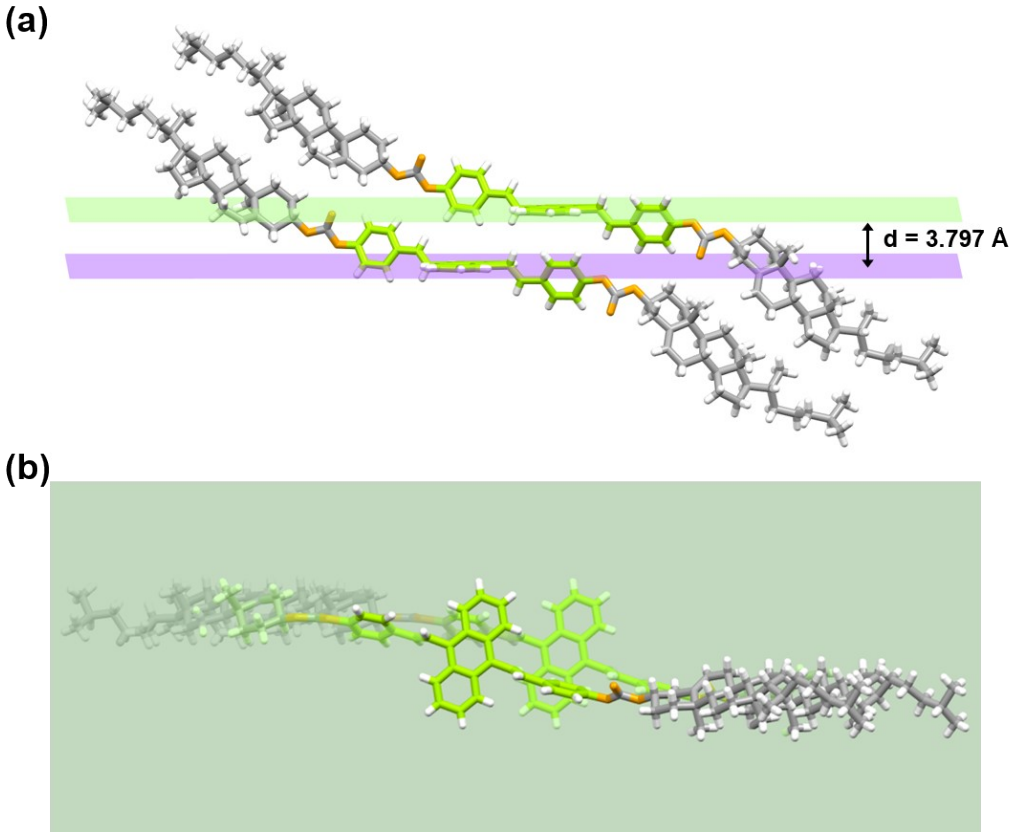

Fig. S24 (a) Side view and (b) top view with the central anthracene moiety as the reference plane.

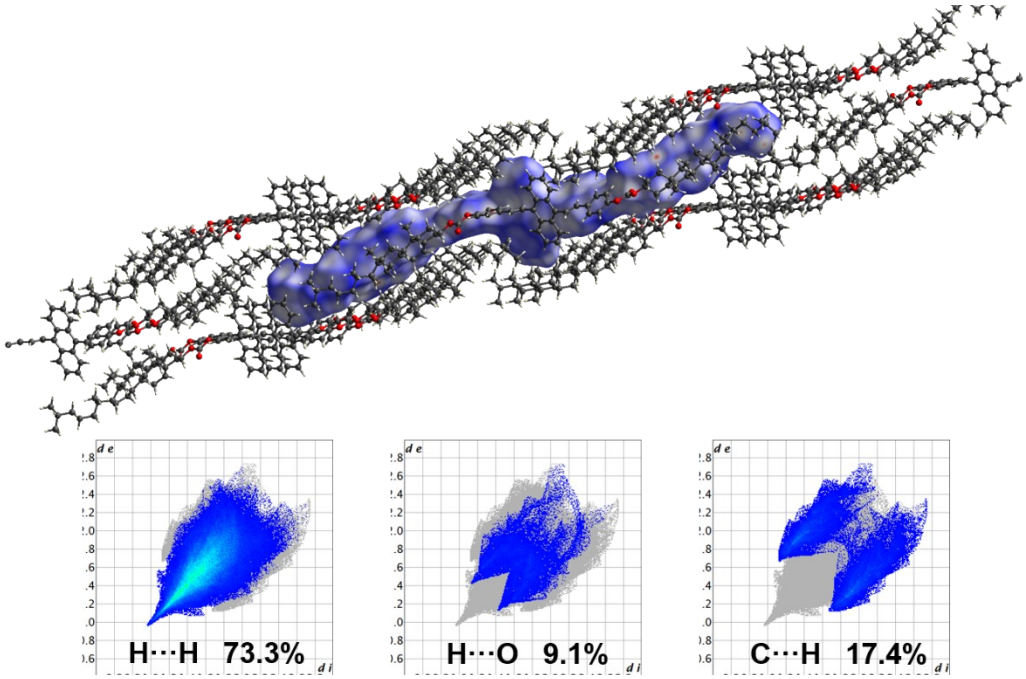

Fig. S25 Hirshfeld surface analysis of the DSA-Chol single crystal and fingerprint plots of different intermolecular interactions.

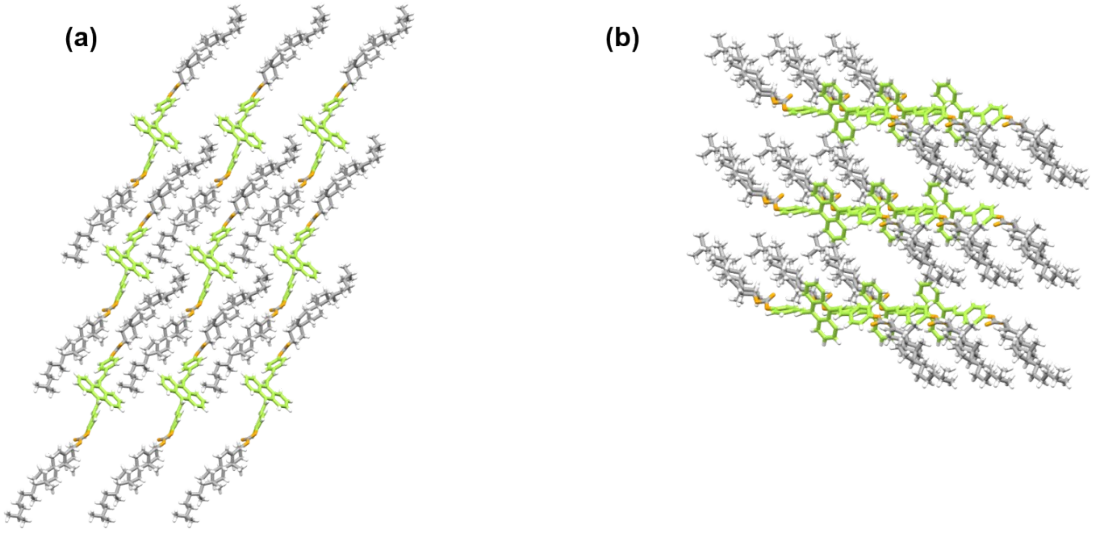

Fig. S26 Molecular packing mode of the crystal viewed along the (a) a-axis and the (b) c-axis.

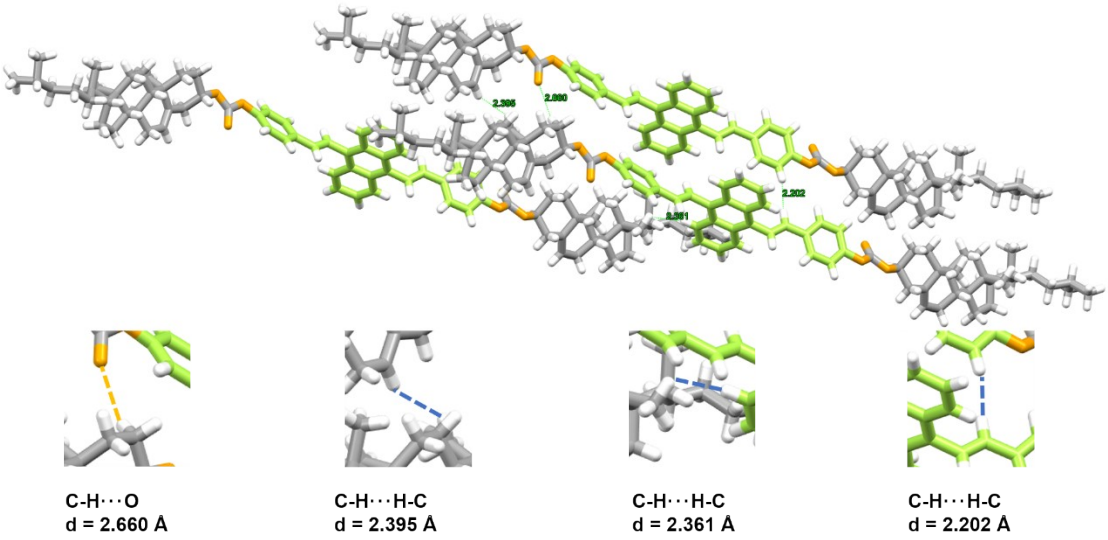

Fig. S27 Intermolecular interactions within the single crystal.

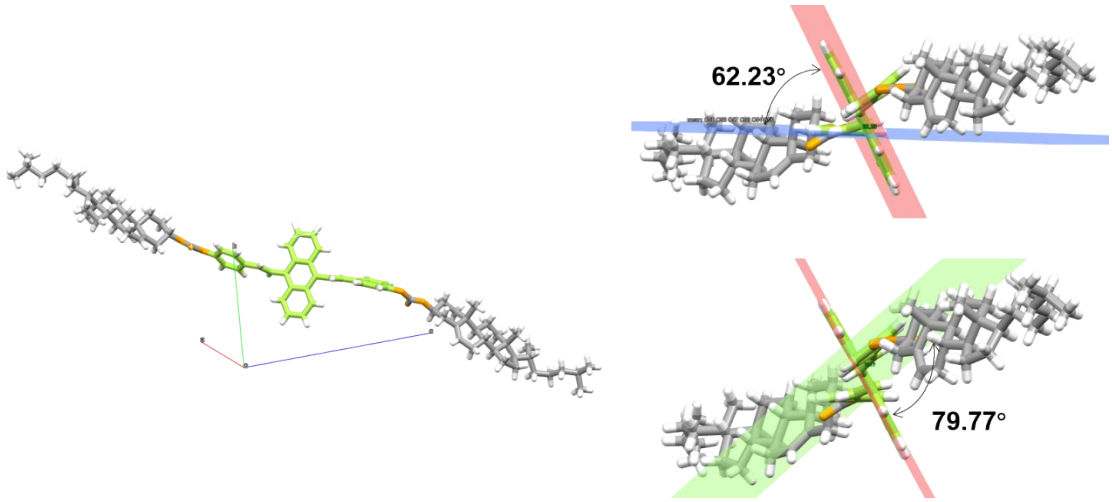

Fig. S28 Dihedral angles between the central anthracene unit and the styryl groups on both sides of the DSA moiety.

Table. S3 Single crystal structure and refinement parameters

Name	DSA-Chol
empirical formula	$C_{86}H_{110}O_6$
formula wt	1239.73
T [K]	293
crystal system, space group	P 1
a [Å]	7.1333(9)
b [Å]	12.7580(19)
c [Å]	20.093(3)
α [deg]	102.376(4)
β [deg]	90.215(4)
γ [deg]	94.854(4)
V [Å^3]	1779.3(4)
Z	1
F (000)	674.0
density, Mg/m^3	1.157
μ [mm^{-1}]	0.070
θ range [deg]	2.820-26.150
no. of reflections collected	18148
no. of unique reflections	10699
R (int)	0.0476
Good-of-fit on F^2	1.053
R_1 [$I>2\sigma(I)$]	0.0688
ωR_2 [$I>2\sigma(I)$]]	0.1905
R_1 (all data)	0.0717
ωR_2 (all data)	0.1968

4. Supporting references.

1. Y. Zhang, Y. Chen, X. Li, J. Zhang, J. Chen, B. Xu, X. Fu and W. Tian, *Polymer Chemistry*, 2014, **5**, 3824-3830.
2. Gaussian 16, Revision A.03, M. J. Frisch, G. W. Trucks, H. B. Schlegel, G. E. Scuseria, M. A. Robb, J. R. Cheeseman, G. Scalmani, V. Barone, G. A. Petersson, H. Nakatsuji, X. Li, M. Caricato, A. V. Marenich, J. Bloino, B. G. Janesko, R. Gomperts, B. Mennucci, H. P. Hratchian, J. V. Ortiz, A. F. Izmaylov, J. L. Sonnenberg, D. Williams-Young, F. Ding, F. Lipparini, F. Egidi, J. Goings, B. Peng, A. Petrone, T. Henderson, D. Ranasinghe, V. G. Zakrzewski, J. Gao, N. Rega, G. Zheng, W. Liang, M. Hada, M. Ehara, K. Toyota, R. Fukuda, J. Hasegawa, M. Ishida, T. Nakajima, Y. Honda, O. Kitao, H. Nakai, T. Vreven, K. Throssell, J. A. Montgomery, Jr., J. E. Peralta, F. Ogliaro, M. J. Bearpark, J. J. Heyd, E. N. Brothers, K. N. Kudin, V. N. Staroverov, T. A. Keith, R. Kobayashi, J. Normand, K. Raghavachari, A. P. Rendell, J. C. Burant, S. S. Iyengar, J. Tomasi, M. Cossi, J. M. Millam, M. Klene, C. Adamo, R. Cammi, J. W. Ochterski, R. L. Martin, K. Morokuma, O. Farkas, J. B. Foresman, and D. J. Fox, Gaussian, Inc., Wallingford CT, 2016.
3. (a) T. Lu and F. Chen, *Journal of Computational Chemistry*, 2012, **33**, 580-592; (b) T. Lu, *The Journal of Chemical Physics*, 2024, **161**, 082503.
4. C. Tu, W. Wu, W. Liang, D. Zhang, W. Xu, S. Wan, W. Lu and C. Yang, *Angewandte Chemie International Edition*, 2022, **61**, e202203541.